Research Article | Vol. 28, No. 20 / 28 September 2020 / Optics Express 29054
Optics EXPRESS

Femtosecond laser fabrication of monolithic double volume phase-gratings in glass

J. J. Azkona,[1,2] M. Gómez-Aranzadi,[1,2] A. Rodriguez,[1,2] T. Morlanes,[3] J. L. de la Peña,[3] and S. M. Olaizola[1,2,*]

[1] CEIT-Basque Research and Technology Alliance (BRTA), Manuel Lardizabal 15, 20018 Donostia / San Sebastián, Spain
[2] Universidad de Navarra, Tecnun, Manuel Lardizabal 13, 20018 Donostia / San Sebastián, Spain
[3] Fagor Aotek S. Coop., Paseo Torrebaso 4, 20540 Eskoriatza, Spain
[*] yolaizola@ceit.es

Abstract: A diffractive optical element was fabricated by monolithically integrating two volume phase-gratings (VPGs) in the bulk of a single-piece transparent material. A computer model of the diffraction generated by the double volume phase-grating (DVPG) was made with a rigorous coupled wave analysis simulator. Simulations and experiments show that the diffractive behavior of a DVPG can be controlled by arranging the relative displacement and the distance between the VPGs according to Talbot self-imaging planes. In order to diffract the total incident light, the phase accumulation in the VPGs has to be $\pi/2$, which was achieved by single-scan femtosecond laser processing of a nanocrystal doped glass as the substrate material. *Ex situ* microscope images of the cross-sections are presented for laser processed lines in the form of VPGs and DVPGs. The far-field diffraction of DVPGs formed by selectively located VPGs was characterized with a monochromatic 633 nm and a supercontinuum white light. Functional designs of high diffraction efficiency with potential applications in photonics were successfully fabricated in a one-step and free of chemicals process.

1. Introduction

Femtosecond laser processing of transparent materials has an increasing potential to be applied in the fabrication of diffractive optical elements (DOEs). This technology has different advantages that can lead manufacturers of DOEs to choose it as their fabrication technology; first, it provides a straightforward manufacturing process for volume fabrication of DOEs, which can be more adequate than surface-fabricated DOEs in a variety of cases. Some examples include applications in environments where a high risk of surface damage is possible, i.e. industrial applications, or the need to provide DOEs with advanced functionalities, like higher diffraction orders, form-birefringence or high diffraction efficiency Bragg gratings [1,2]. Furthermore, within the fabrication methods of volume DOEs, femtosecond direct writing offers a higher robustness, 3D operation malleability, and variety of substrate materials than other fabrication techniques such as laser interference patterning [3]. Reports concerning femtosecond laser fabrication of volume phase-gratings (VPGs) [4–10], Fresnel lenses [11–13], form-birefringence [14] or optical-holographic imaging [15,16] have increased during the last decades, which contribute to the state of the art in spatial and spectral beam shaping, beam splitting and combining, optical imaging and data storage [17].

The amount of the refractive index change generated in the laser-processed zone is one of the most limiting factors when a DOE is fabricated using femtosecond laser direct writing. When the top index modification is limited below 10^{-3}, which is typical in a wide range of materials [18–20], functional DOEs can be fabricated by compensating the low refractive index change with more scanning repetitions. The first approach for increasing the efficiency of the DOEs with this method was the fabrication of cascade multi-layered gratings [5,7,8,10]. The assumption

#402275 https://doi.org/10.1364/OE.402275
Journal © 2020 Received 9 Jul 2020; revised 21 Aug 2020; accepted 22 Aug 2020; published 15 Sep 2020

Optics EXPRESS

when using this fabrication technique is that the overlapped regions between separated laser scans generate a negligible change that can be treated as a continuous modification [9]. High diffraction VPGs of up to 90% efficiency have been accomplished with this method. Nevertheless, as these VPGs behave like Bragg gratings [21], they have the disadvantage that this high performance is only achieved when the VPG is illuminated at the Bragg condition [22,23]. In particular, this can limit the application of such VPGs in setups where perpendicular illumination is needed, or setups where VPGs are illuminated at several wavelengths.

Some authors have studied a different approach of multilayer fabrication in order to potentially improve the efficiency of VPGs outside the above mentioned specific configuration [10,24,25]. This fabrication approach is based on the fabrication of separated layers where the layer-to-layer distance coincides with the Talbot self-imaging planes. In this manner, when the laser-modified elements are coherently layered with the respective near-field diffraction pattern, an enhancement of the total diffraction efficiency is achieved. In the case of Ng *et al.* [24], a combined 1st order diffraction efficiency of up to 35% was achieved when 8 layers were separately inscribed with a distance of 20 μm between them. Some other authors have reported the fabrication of VPGs with even more complex geometrical arrangements, such as the stitching of layers with relative displacement [10], or the variation of grating orientation between the respective layers [25].

To the best of our knowledge, the fabrication method of selectively inscribing a number of separated volume phase-gratings has been only tested with VPGs at a high resolution limit ($\Lambda \sim 1$ μm period) and small phase accumulation (combined 1st diffraction efficiency of a single-grating of up to 5.2%). In this work, the fabrication of separated phase elements was investigated in a larger size approach. VPG periods of $\Lambda = 10$ μm allowed us to fabricate single-gratings of a combined efficiency of the 1st diffraction orders up to 42.3%. This regime of single-layer VPGs with a high diffraction efficiency led us to the functional development of double volume phase-gratings (DVPGs) with hundreds of microns of distance between the phase elements. Double-grating systems are usually found in reflective or transmission configuration in applications such as spectroscopy [26], interferometry [27], laser pulse compression [28], or metrology [29], but they are usually found like a combined system of separated elements. In this work, we propose the implementation of a grating pair that is monolithically integrated in a single piece of bulk material. Due to the two dimensional light modulation given in the Talbot effect, the fabrication of the DVPGs was optimized both in the distance and the relative displacement between the gratings. Such structures have been fabricated in a borosilicate glass doped with CdS_xSe_{1-x} semiconductor nanocrystals (OG530, Schott Glass Inc.), a material known for showing a high refractive index change when processed with femtosecond laser [30].

2. Methods

The fabrication of the DVPGs [Fig. 1(a)] was made with an Amplitude Satsuma Laser, consisting of a 500 kHz diode-pumped ultrafast fiber amplifier system of $\lambda = 1030$ nm and 280 fs pulse duration. The laser beam at the output aperture of the amplifier is a Gaussian of $M^2 = 1.2$ and 2.7 mm of diameter. A beam expander of 3x was used to expand the diameter of the beam and fill the total aperture of the focusing objective, which is a high power NIR laser objective with an entrance aperture of 8 mm and a NA of 0.4. In the focus of the objective lens the spot size is 2.5 μm, according to the specifications of the suppliers. Then, a computer controlled scanning system of motorized linear stages was used to fabricate structures along the 3-axes x, y and z inside the bulk material. DVPGs were fabricated following the fabrication strategy in the scheme Fig. 1 b); both VPGs in the DVPG were fabricated simultaneously by making a two depth inscription in each lateral step. Every VPG and DVPG presented in this work was fabricated with a period of $\Lambda = 10$ μm.

A borosilicate glass doped with a 1% volume fraction of embedded CdS_xSe_{1-x} semiconductor nanocrystals of 3.9 nm radius (OG530 Schott Glass Inc.) was used as the substrate material. Its

Optics EXPRESS

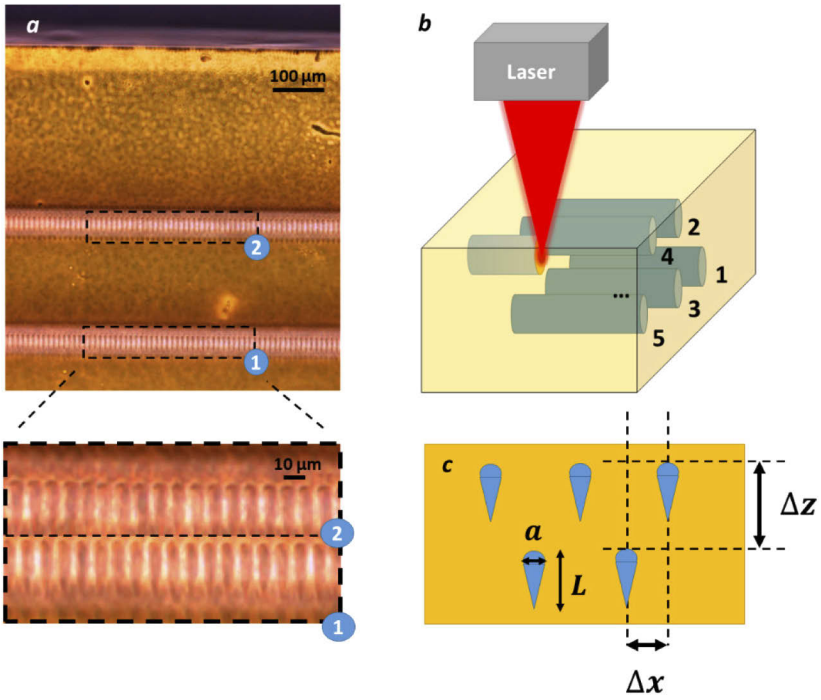

Fig. 1. a) Cross-section microscope image (10x) of a double volume phase-grating fabricated in the nanostructured glass with a femtosecond laser. b) Scheme of the laser fabrication strategy followed in this work. c) Droplet shape approximation taken for the simulation with the RCWA numerical solver. The definitions of the widths a and thickness L, together with the relative displacement Δx and the distance between the gratings Δz are illustrated.

refractive index in the range from 550 nm to 850 nm is 1.51. This material is extensively use as an optical cut-off color filter, and for that reason has an orange colored appearance.

A numerical rigorous coupled wave analysis (RCWA) software (GSOLVER) was used in order to simulate the far-field diffraction generated by the DVPGs. The profile shape of the phase element was approximated by a droplet shape [Fig. 1(c)] formed with a triangle and a semicircle. The refractive index change Δn is assumed to be homogeneous inside the structure. This value can be interpreted as the averaged value of the actual Δn distribution [30,31] in the laser modified zone. This approximation is expected to be adequate as long as the thickness parameter Q of the gratings is less than unit [32]. In order to fit with the experimental measurements, the losses generated from reflections and absorption were introduced in the model by multiplying the simulated efficiency results by a factor of 0.8. This value can be approximately subdivided in scattering and absorption losses of 12% and surface reflection losses of 8%.

Laser processed areas were characterized by an optical microscope with magnifications of 10x and 40x. The images presented in the work have been taken after cleaving the sample in a direction transversal to the laser inscribed lines. In order to distinguish the cross-section image from the roughness of the surrounding material, oil was applied to fill the roughness of the surface. A HeNe $\lambda = 633$ nm and a supercontinuum white light laser were used to measure the far-field diffraction efficiencies. Diffracted beam intensities were measured by both a manual potentiometer (for the monochromatic laser) and a spectrometer Oriel MS257 with an integrating sphere.

Optics EXPRESS

3. Results

3.1. Single volume phase-grating fabrication

Laser processing conditions were optimized in order to fabricate single layer VPGs. Microscope images of the laser-processed cross-sections at different pulse energies are presented in Fig. 2(a). A repetition rate of 500 kHz was selected at a scanning speed of 2 mm/s. Widths *a* ranging from 2.5 µm to > 10 µm and thicknesses L from 14.6 µm to 41.9 µm are measured (widths are taken in the equator of the droplet). Measurements of laser modified zones wider than the laser spot size (~ 2.5 µm) suggest that heat accumulation is occurring [33–35]. An overall droplet shape is observed, which gets more pronounced as the pulse energy increases, with the shape size increasing with laser pulse energy. This indicates a larger area of multiphoton ionization [36,37]. Microscope images of the laser modified zone appear homogeneously dark, which could be explained by the redshift in the absorption spectra of the nanocrystals [38]. The surrounding grey region suggests that an overlapped molten region has been generated as VP Gs of $\Lambda = 10\mu m$ were fabricated. This means that the refractive index that surrounds the droplet shapes could be different [39] from the rest of the bulk, which in principle could affect the amplitude of the phase modulation.

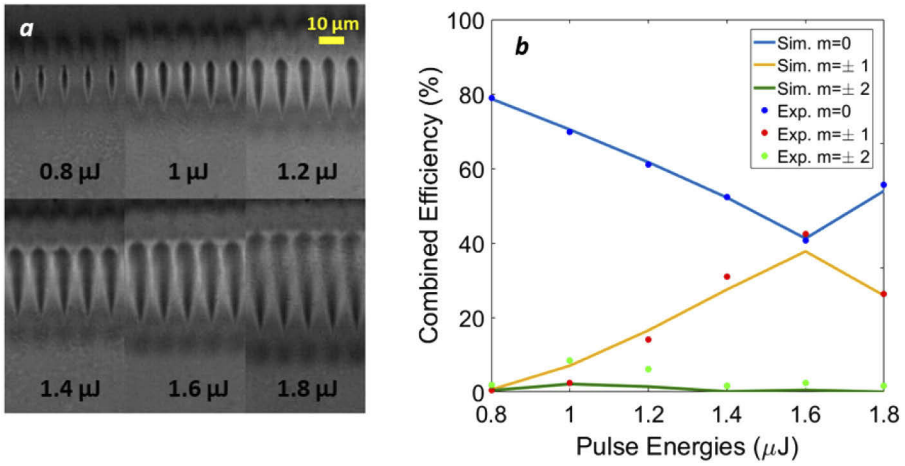

Fig. 2. a) Optical microscope images of the cross-sections of the laser inscribed lines at different pulse energies (40x magnification). b) Experimental and simulated far-field diffraction efficiencies of VPG fabricated at different pulse energies. Simulations were done by taking the dimensions of the laser modified zones observed in the microscope cross-sections. The refractive index changes implemented in the simulations for each pulse energy are $\Delta n = 0.003$, $\Delta n = 0.0055$, $\Delta n = 0.006$, $\Delta n = 0.0065$, $\Delta n = 0.0075$ and $\Delta n = 0.0055$. The combined efficiency is shown meaning that both sides ± for each diffraction order have been summed. Experimental and simulated results were obtained at $\lambda = 633$ nm and perpendicular illumination.

Far-field diffraction efficiencies of single layer VPGs fabricated at different pulse energies are presented in the Fig. 2(b). In the image, measured efficiencies (points) are compared with RCWA simulated efficiencies (lines). In order to simulate the efficiencies, the droplet like structure in Fig. 1(c) was adapted to the measured widths and thicknesses in Fig. 2(a). Refractive index changes Δn going from 0.003 to 0.0075 give a good agreement between simulations and experiments. A maximum combined 1st order efficiency of 42.3% is achieved when the pulse energy is 1.6 µJ (L = 34.2 µm and $\Delta n = 0.0075$). The 2nd order diffraction efficiency remains small comparing with the 1st order efficiency as expected for a VPG. This value is equivalent to

Optics EXPRESS

a VPG of $\Delta\varphi = \pi/2$ using the planar grating approximation [21]. The increasing widths of the laser modified zone can lead to a reduction of the diffraction efficiency of the non-zero orders efficiency [35] for the VPG fabricated at 1.8 μJ.

3.2. Double volume phase-grating fabrication

The cross-section images of DVPGs fabricated at 1.2 μJ and 1.6 μJ are presented in Fig. 3. The sections of both DVPGs are well-defined. The fabrication strategy that we have followed is depicted in the scheme in the Fig. 1(b). In the Table 1, thicknesses of the DVPGs cross-sections have been compared with separated VPGs fabricated at the same exact conditions, i.e., the same depths, pulse energies and scanning speeds. The measured distances between the gratings are $\Delta z = 242.4$ μm and $\Delta z = 244.2$ μm respectively. A small deviation is observed between the VPGs fabricated in the deeper layer (VPG2) when fabricated separately and assembled in DVPGs. This is produced because the upper structures in z ~ 200 μm (VPG1) fade the focusing of the pulse during the fabrication process thus leading to a smaller laser modified zone.

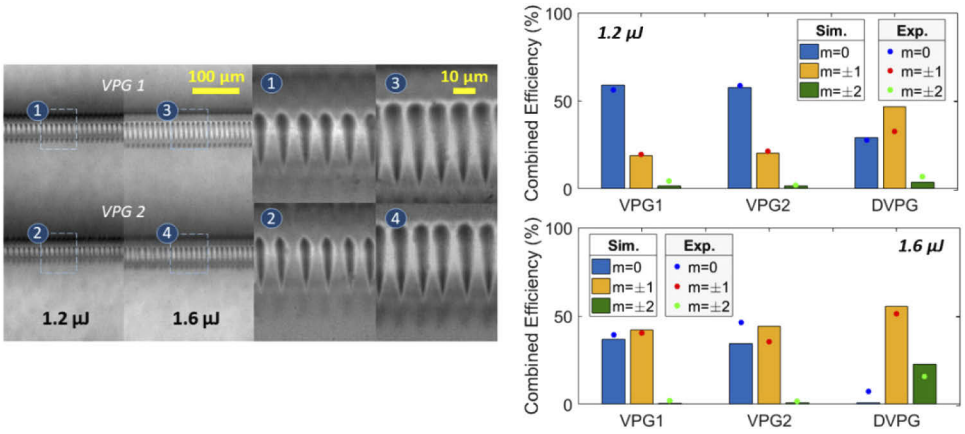

Fig. 3. Microscope images of the cross-sections of two DVPGs fabricated at 1.2 μJ and 1.6 μJ pulse energies, 500 kHz, 2 mm/s, at depths of ~ 200 μm and ~ 440 μm. Images were taken at 10x and 40x magnification. Experimental and simulated combined diffraction efficiency of separated VPGs and DVPG at 1.2 μJ and 1.6 μJ are shown. RCWA simulations were done by taking the dimensions measured from the microscope image (listed in Table 1) and $\Delta n = 0.006$ and $\Delta n = 0.0075$, respectively. Experimental and simulated results were obtained at $\lambda = 633$ nm and perpendicular illumination.

Table 1. Thicknesses of separately fabricated VPGs and DVPGs

1.2 μJ				1.6 μJ			
	Thickness (μm)				Thickness (μm)		
Depth (μm)	VPG1	VPG2	DVPG	Depth (μm)	VPG1	VPG2	DVPG
214.7 ± 0.5	25.8 ± 0.4	-	25.5 ± 0.4	199 ± 1.4	36.6 ± 0.5	-	36.1 ± 0.5
457.1 ± 0.8	-	26.7 ± 0.6	23.4 ± 0.3	443.2 ± 0.8	-	37.9 ± 0.2	31.8 ± 0.4

Measured and simulated diffraction efficiencies of the separated VPGs and DVPG are shown in Fig. 3. VPGs individually fabricated at the same conditions were separately characterized and then fabricated and characterized assembled into DVPGs. A good agreement between the experimental and simulated results are obtained, both for the separated VPGs and the DVPGs. The dimension sizes for the simulations were taken from the cross-section images in Table 1 and

Optics EXPRESS

the refractive index changes are those used in Fig. 2(b) for 1.2 μJ and 1.6 μJ, *i.e.*, $\Delta n = 0.006$ and $\Delta n = 0.0075$. The experimental results obtained in DVPGs with these refractive index changes are in good agreement with the results of the simulations, further validating the chosen values. First order diffraction efficiency of single VPGs fabricated at 1.2 μJ and 1.6 μJ are respectively 20.4% and 40.8%, which are equivalent to a phase accumulation of $\Delta\varphi = \pi/3$ and $\pi/2$, respectively. It is observed that the diffraction efficiency is improved when both VPGs are assembled into the DVPG. A higher loss is observed in the 1st diffraction order efficiency for the DVPG fabricated at 1.2 μJ comparing with the simulated theoretical value. Regarding the 0th diffraction order, theoretically almost a total vanishing of the 0th order can happen when the phase accumulation in both gratings is $\Delta\varphi = \pi/2$. Experimentally, a diffraction value of 8% was measured with the DVPG fabricated at 1.6 μJ.

Figure 4 shows the diffraction efficiencies of DVPGs when Δx and Δz are varied. The distances between the gratings Δz was varied from 215 μm to 280 μm in two configurations of relative displacement; $\Delta x = 0$ μm and at $\Delta x = \Lambda/2 = 5$ μm. These values were chosen in order to generate a symmetrical diffraction pattern. Distance from the glass surface to the first grating was kept constant at $z = 200$ μm, and relative displacement between the gratings was measured from microscope cross-section images. In this case DVPGs were fabricated at 1.6 μJ pulse energy. Experimental results are depicted together with the RCWA simulated results at equivalent conditions.

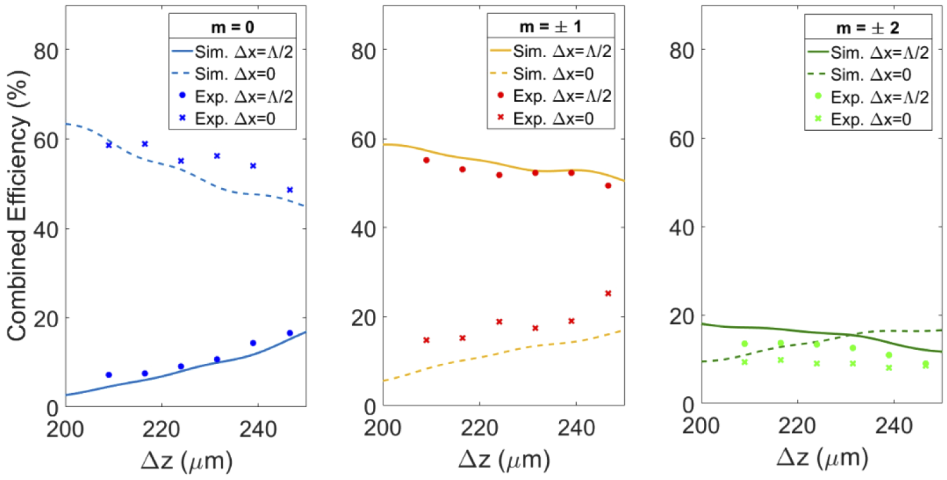

Fig. 4. Experimental and simulated far-field efficiencies at $m = 0$, $m = \pm 1$ and $m = \pm 2$ diffraction orders of DVPGs fabricated at different distances Δz, for a relative displacement of $\Delta x = 0$ and $\Delta x = \Lambda/2$. DVPGs were fabricated at 1.6μJ. Distances between the VPGs were measured from microscope images. RCWA simulations were done with the droplet profile and sizes taken for VPG fabricated at 1.6μJ, width of $a = 8$μm, thickness $L = 36$μm and the refractive index change was $\Delta n = 0.0075$. Experimental and simulated results were obtained at $\lambda = 633$ nm and perpendicular illumination.

Figure 4 shows that the 0th and 1st diffraction efficiencies are drastically affected by the change of Δx. At the 0th order, the efficiencies are 59% and 7.3% respectively for $\Delta x = 0$ and $\Delta x = \Lambda/2$. Similar but inverse efficiencies are obtained at the 1st order, where the efficiencies are 14.8% and 55.2% respectively for $\Delta x = 0$ and $\Delta x = \Lambda/2$. This behaviour can be explained by the near-field propagation generated between the gratings. Our hypothesis is that, as the light distribution in the second grating is determined by the Talbot effect generated by the first grating, a constructive or destructive interference can be generated. Regarding the distance between gratings, in an ideal case RCWA simulations of almost planar DVPGs of $\Delta n = 0.16$ and $L = 1$ μm show a strong

Optics EXPRESS

dependence of the diffraction on Δz. For the case of Δx =Λ/2 in particular, a 80% of the combined 1st diffraction efficiency is achieved when the distance between the gratings is very close to $Z_T/2$, where $Z_T = 2n\Lambda^2/\lambda_0 = 477$ μm is the Talbot distance inside the glass. As the phase element profile gets thicker and less rectangular, the dependency on Δz starts to fade.

3.3. Angular and spectral characterization of DVPGs

The thickness parameter Q [32] of a single VPG fabricated at 1.6μJ [Fig. 2(a)] is less than a unit, and therefore, it is expected to behave like a thin-grating. Experiments have shown that the diffraction efficiency of a single VPG of this kind has a small dependence on the angle of incidence. For a range going from – 4 ° to 4 °, the 0th order efficiency is maintained almost constant at a ~ 50%, and the combined 1st order efficiency varies around the ~ 36%, with small asymmetries between the ± sides of the diffraction pattern. Figure 5 shows the dependence of a DVPG when illuminated with different angles of incidence. In contrast with the diffraction of a single VPG, a strong dependence on the angle of incidence is observed. Furthermore, this dependence is different from dependence of the diffraction on the angle of incidence observed in a Bragg grating [7–9], where the maximum efficiency is achieved at the blazed angle. In the case of DVPGs, a maximum diffraction is achieved when the illumination is perpendicular. A simulated DVPG with the droplet phase profile and a Δn = 0.007 fits well with the experimental results. Snell's law in the glass interface was taken into account in order to compare with experimental results. New losses in the glass interfaces because of the variation of the angle of incidence have been accounted and are negligible. A 0th order efficiency of 5.1% and a combined 1st order efficiency of 53% is achieved at perpendicular illumination. At the same time, a second maximization cycle is observed close to ± 4 °, where minimization is given at ± 2 °. These cycles could be explained by the variation of the Talbot effect when the angle of incidence is not perpendicular. The diffraction in the order m = -1 fits better with the simulated results than the m = 1 order, which could be explained by the asymmetrical behavior already observed in the single VPG diffraction fabricated at 1.6 μJ.

In order to study the dependence of the diffraction on the illumination wavelength, DVPGs formed with multilayered VPGs were fabricated at different distances (Δz) between the gratings from 209 μm to 239 μm and a relative displacement of Δx = Λ/2. The laser processing conditions were 500 kHz, pulse energy of 1.6 μJ and a scanning speed of 2 mm/s. In order to enhance the phase accumulation for long wavelengths, since phase accumulation should be close to Δϕ =π/2 (as displayed in Fig. 3), each VPG in the DVPG was fabricated by overlapping two layers in the z axis with a step difference of 10 μm. In this manner, the effective thickness of each grating increases by several microns. In order to incorporate this to the RCWA simulations, the thickness of the droplet shape [shown in Fig. 2(a)] was extended to 40 μm. The refractive index change implemented in the simulations was Δn = 0.0075. The illumination white light source was impinged perpendicular to the DVPG. The dependence of the combined 1st order diffraction generated by a DVPG on the illumination spectrum is shown in Fig. 6.

Figure 6 shows the combined 1st efficiency close to the peak of diffraction generated at different wavelengths. It can be observed that the peak wavelength depends on the distance between the gratings. Similar peak efficiencies of ~ 63% are measured at λ = 827 nm, λ = 794 nm and λ = 751 nm for Δz = 209 μm, Δz = 224 μm and Δz = 239 μm. Notice that as the distance between the gratings increases, the peak wavelengths is inversely reduced, which could be explained by the inverse dependence of the Talbot distance on the wavelength. As RCWA simulation with almost planar VPGs show that maximum efficiency is achieved when the Δz coincide with the half Talbot distance, control of the peak wavelength can be predicted. In order to do this, the Δn or the L of the phase element has to be optimized for achieving a Δϕ =π/2 at different wavelengths. Thus, almost planar simulations have shown an agreement of ± 20 nm with predicted peak wavelength. In the case of the droplet profile as in Fig. 6, simulations and experimental results show a good

Optics EXPRESS

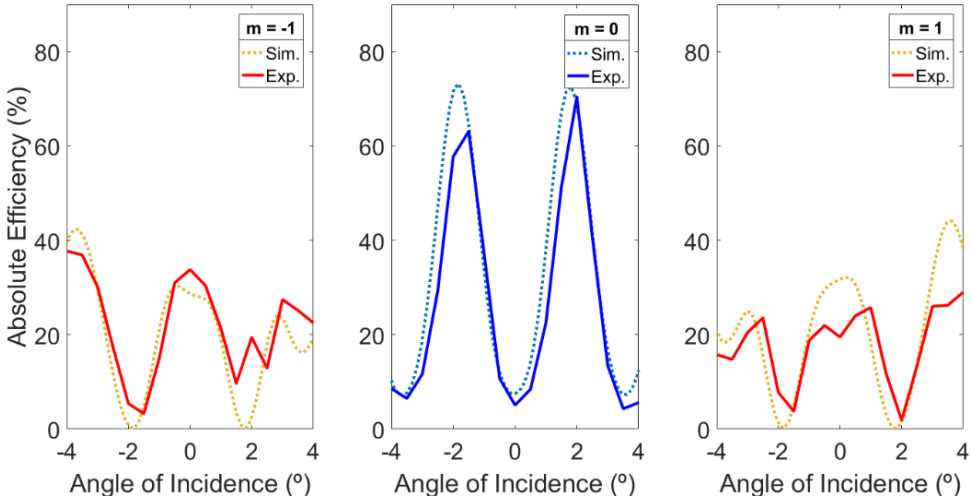

Fig. 5. Experimental and simulated far-field diffraction efficiencies at the orders m = -1, m = 0 and m = 1 of a DVPG when the angle of incidence is variated. A DVPG with a $\Delta x = \Lambda/2$ and a $\Delta z = 244.2\mu m$ was fabricated at 1.6μJ, 500 kHz and a scanning speed of 2 mm/s. Experimental measurements were taken by changing the angle of incidence in steps of 0.5 °. In order to see asymmetrical effects, 1st diffraction orders are shown for both sides (+1 and -1). RCWA simulations were done with droplet elements with $a = 8\mu m$ width, $L = 30\mu m$ thickness and $\Delta n = 0.007$. Experimental and simulated results were obtained illuminating at $\lambda = 633$ nm.

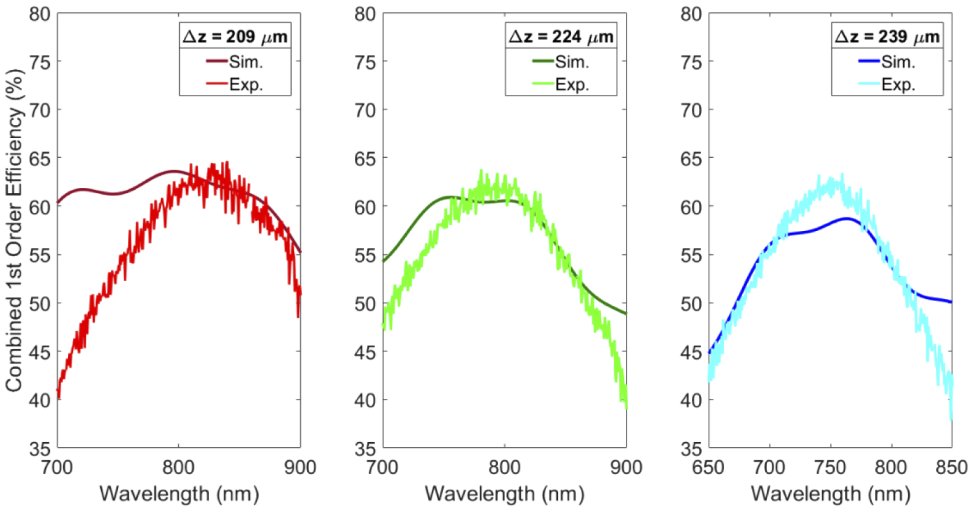

Fig. 6. Experimental and simulated far-field diffraction efficiency of the combined 1st order of a DVPG when illuminated at different wavelengths. DVPGs were fabricated by overlapping two layers of gratings in each VPG, with a $\Delta x = \Lambda/2$ and varying the Δz. DVPGs were fabricated at 1.6μJ, 500 kHz and a scanning speed of 2 mm/s. The white light source was impinged perpendicularly to the DVPG. RCWA simulations were done with a droplet profile of $a = 8\mu m$ width, $L = 40$ μm thickness and $\Delta n = 0.0075$.

agreement for a spectral width of $\Delta\lambda = 200$ nm. Nevertheless, as these VPGs are not planar and

Optics EXPRESS

phase accumulation $\Delta\phi$ has not been optimized for the different wavelengths, the correspondence between the peak wavelength and the Δz given by the half Talbot distance is faded.

4. Conclusions

Monolithic fabrication of double volume phase-gratings has been successfully achieved using a femtosecond laser. We have presented a new regime of laser integration of medium-sized volume phase-gratings, where single VPGs of combined 1st diffraction efficiency of 42.3% were the building blocks to fabricate the DVPGs. Laser induced modifications have been structured with a separation of hundreds of microns, which to the best of our knowledge, is a novel approach that can push further the possibilities of laser fabrication of volume DOEs. By doing this, an improvement of the diffraction effect has been observed with no restriction of blazed angles. The agreement between the simulations and the experimental data have shown that this effect can be optimized when the distance between the gratings coincide with half the Talbot distance. Furthermore, it has been proven that DVPGs can be optimized for different wavelengths if the distance between the gratings is controlled. 1st order efficiencies of up to 63% were measured at wavelengths in the range between $\lambda = 750$ nm and $\lambda = 830$ nm. Considering that the number of laser scanning repetitions needed in this method are significantly reduced in comparison with the repetitions needed for the fabrication of cascade multilayered VPGs, we conclude that these DVPGs are a promising alternative for a cost-effective solution to fabricate embedded transmission gratings.

Funding

Horizon 2020 Framework Programme (820661).

Acknowledgments

Theoretical support was provided by Luis Miguel Sanchez-Brea, Complutense University of Madrid.

Disclosures

The authors declare no conflicts of interest.

References

1. C. Yang and P. Yeh, "Form birefringence of volume gratings in photopolymers," Appl. Phys. Lett. **69**(23), 3468–3470 (1996).
2. L. B. Glebov, "Volume holographic elements in a photo-thermo-refractive glass," J. Hologr. Speckle **5**(1), 77–84 (2009).
3. B. Robertson, C. Godsalve, and M. R. Taghizadeh, "Dichromated gelatin holography: an investigation into laser-induced damage," Appl. Opt. **32**(33), 6587 (1993).
4. L. Sudrie, M. Franco, B. Prade, and A. Mysyrowicz, "Writing of permanent birefringent microlayers in bulk fused silica with femtosecond laser pulses," Opt. Commun. **171**(4-6), 279–284 (1999).
5. K. Yamada, W. Watanabe, K. Kintaka, J. Nishii, and K. Itoh, "*Fabrication of volume grating induced in silica glass by femtosecond laser*," in I. Miyamoto, A. Ostendorf, K. Sugioka, and H. Helvajian, eds. (International Society for Optics and Photonics, 2003), 5063, p. 474.
6. C. Florea and K. A. Winick, "Fabrication and characterization of photonic devices directly written in glass using femtosecond laser pulses," J. Lightwave Technol. **21**(1), 246–253 (2003).
7. D. Lee, R. R. Thomson, and C. R. Cunningham, "Performance of volume phase gratings manufactured using ultrafast laser inscription," in *Modern Technologies in Space- and Ground-Based Telescopes and Instrumentation II*, R. Navarro, C. R. Cunningham, and E. Prieto, eds. (SPIE, 2012), 8450, p. 84502X.
8. D. G. MacLachlan, R. R. Thomson, C. R. Cunningham, and D. Lee, "Mid-Infrared Volume Phase Gratings Manufactured using Ultrafast Laser Inscription," Opt. Mater. Express **3**(10), 1616 (2013).
9. M. Mikutis, T. Kudrius, G. Šlekys, D. Paipulas, and S. Juodkazis, "High 90% efficiency Bragg gratings formed in fused silica by femtosecond Gauss-Bessel laser beams," Opt. Mater. Express **3**(11), 1862 (2013).

Optics EXPRESS

10. J. Liu, Z. Zhang, Z. Lu, G. Xiao, F. Sun, S. Chang, and C. Flueraru, "Fabrication and stitching of embedded multi-layer micro-gratings in fused silica glass by fs laser pulses," Appl. Phys. B **86**(1), 151–154 (2006).
11. E. Bricchi, J. D. Mills, P. G. Kazansky, B. G. Klappauf, and J. J. Baumberg, "Birefringent Fresnel zone plates in silica fabricated by femtosecond laser machining," Opt. Lett. **27**(24), 2200 (2002).
12. W. Watanabe, D. Kuroda, K. Itoh, and J. Nishii, "Fabrication of Fresnel zone plate embedded in silica glass by femtosecond laser pulses," Opt. Express **10**(19), 978 (2002).
13. K. Yamada, W. Watanabe, Y. Li, K. Itoh, and J. Nishii, "Multilevel phase-type diffractive lenses in silica glass induced by filamentation of femtosecond laser pulses," Opt. Lett. **29**(16), 1846 (2004).
14. Y. Shimotsuma, P. G. Kazansky, J. Qiu, and K. Hirao, "Self-Organized Nanogratings in Glass Irradiated by Ultrashort Light Pulses," Phys. Rev. Lett. **91**(24), 247405 (2003).
15. B. Jia, J. Serbin, H. Kim, B. Lee, J. Li, and M. Gu, "Use of two-photon polymerization for continuous gray-level encoding of diffractive optical elements," Appl. Phys. Lett. **90**(7), 073503 (2007).
16. Y. Shimotsuma, M. Sakakura, P. G. Kazansky, M. Beresna, J. Qiu, K. Miura, and K. Hirao, "Ultrafast manipulation of self-assembled form birefringence in glass," Adv. Mater. **22**(36), 4039–4043 (2010).
17. D. C. O'Shea, T. J. Suleski, A. D. Kathman, and D. W. Prather, *Diffractive Optics: Design, Fabrication, and Test* (SPIE, 2003).
18. K. Miura, J. Qiu, H. Inouye, T. Mitsuyu, and K. Hirao, "Photowritten optical waveguides in various glasses with ultrashort pulse laser," Appl. Phys. Lett. **71**(23), 3329–3331 (1997).
19. A. M. Streltsov and N. F. Borrelli, "Fabrication and analysis of a directional coupler written in glass by nanojoule femtosecond laser pulses," Opt. Lett. **26**(1), 42 (2001).
20. M. Will, S. Nolte, B. N. Chichkov, and A. Tünnermann, "Optical properties of waveguides fabricated in fused silica by femtosecond laser pulses," Appl. Opt. **41**(21), 4360 (2002).
21. T. K. Gaylord and M. G. Moharam, "Planar dielectric grating diffraction theories," Appl. Phys. B **28**(1), 1–14 (1982).
22. A. Bunkowski, O. Burmeister, T. Clausnitzer, E. B. Kley, A. Tünnermann, K. Danzmann, and R. Schnabel, "Optical characterization of ultrahigh diffraction efficiency gratings," Appl. Opt. **45**(23), 5795–5799 (2006).
23. T. Clausnitzer, T. Kämpfe, F. Brückner, R. Heinze, E.-B. Kley, and A. Tünnermann, "Reflection-reduced encapsulated transmission grating," Opt. Lett. **33**(17), 1972 (2008).
24. M. L. Ng, D. Chanda, and P. R. Herman, "Coherent stitching of light in multilayered diffractive optical elements," Opt. Express **20**(21), 23960 (2012).
25. L. Yuan, M. L. Ng, and P. R. Herman, "Femtosecond laser writing of phase-tuned volume gratings for symmetry control in 3D photonic crystal holographic lithography," Opt. Mater. Express **5**(3), 515 (2015).
26. S. Grabarnik, R. Wolffenbuttel, A. Emadi, M. Loktev, E. Sokolova, and G. Vdovin, "Planar double-grating microspectrometer," Opt. Express **15**(6), 3581 (2007).
27. C. Kappel, A. Selle, M. A. Bader, and G. Marowsky, "Resonant double-grating waveguide structures as inverted Fabry–Perot interferometers," J. Opt. Soc. Am. B **21**(6), 1127 (2004).
28. L. Poletto, F. Frassetto, and P. Villoresi, "Design of an extreme-ultraviolet attosecond compressor," J. Opt. Soc. Am. B **25**(7), B133 (2008).
29. L. M. Sanchez-Brea, F. J. Torcal-Milla, and E. Bernabeu, "Continuous self-imaging regime with a double-grating mask," Appl. Opt. **48**(30), 5722–5727 (2009).
30. R. Martinez-Vazquez, R. Osellame, G. Cerullo, R. Ramponi, and O. Svelto, "Fabrication of photonic devices in nanostructured glasses by femtosecond laser pulses," Opt. Express **15**(20), 12628–12635 (2007).
31. A. Mermillod-Blondin, C. Mauclair, J. Bonse, R. Stoian, E. Audouard, A. Rosenfeld, and I. V. Hertel, "Time-resolved imaging of laser-induced refractive index changes in transparent media," Rev. Sci. Instrum. **82**(3), 033703 (2011).
32. H. Kogelnik, "Coupled Wave Theory for Thick Hologram Gratings," Bell Syst. Tech. J. **48**(9), 2909–2947 (1969).
33. C. B. Schaffer, J. F. García, and E. Mazur, "Bulk heating of transparent materials using a high-repetition-rate femtosecond laser," Appl. Phys. A: Mater. Sci. Process. **76**(3), 351–354 (2003).
34. S. Nolte, M. Will, J. Burghoff, and A. Tünnermann, "Ultrafast laser processing: New options for three-dimensional photonic structures," J. Mod. Opt. **51**(16-18), 2533–2542 (2004).
35. S. M. Eaton, H. Zhang, P. R. Herman, F. Yoshino, L. Shah, J. Bovatsek, and A. Y. Arai, "Heat accumulation effects in femtosecond laser-written waveguides with variable repetition rate," Opt. Express **13**(12), 4708 (2005).
36. P. G. Kazansky, H. Inouye, T. Mitsuyu, K. Miura, J. Qiu, K. Hirao, and F. Starrost, "Anomalous anisotropic light scattering in ge-doped silica glass," Phys. Rev. Lett. **82**(10), 2199–2202 (1999).
37. D. M. Rayner, A. Naumov, and P. B. Corkum, "Ultrashort pulse non-linear optical absorption in transparent media," Opt. Express **13**(9), 3208 (2005).
38. R. Osellame, R. M. Vazquez, G. Cerullo, R. Ramponi, O. Svelto, V. Russo, A. Li Bassi, C. E. Bottani, and C. Spinella, "Interaction between femtosecond laser pulses and CdSxSe1−x quantum dots in glasses," Phys. Rev. B **76**(4), 045340 (2007).
39. S. M. Eaton, H. Zhang, M. L. Ng, J. Li, W.-J. Chen, S. Ho, and P. R. Herman, "Transition from thermal diffusion to heat accumulation in high repetition rate femtosecond laser writing of buried optical waveguides," Opt. Express **16**(13), 9443 (2008).